European Congress on Computational Methods
in Applied Sciences and Engineering (ECCOMAS 2012)
J. Eberhardsteiner et.al. (eds.)
Vienna, Austria, September 10-14, 2012

NUMERICAL SIMULATIONS OF TWO-PHASE FLOW WITH COMFLOW: PAST AND RECENT DEVELOPMENTS

Roel Luppes[1], **Bülent Düz**[2], **Henri J.L. van der Heiden**[1], **Peter van der Plas**[1] **and Arthur E.P. Veldman**[1]

[1]Johann Bernoulli Institute for Mathematics and Computer Science
University of Groningen,
P.O. Box 407, 9700 AK Groningen, The Netherlands
e-mail: {r.luppes,h.j.l.van.der.heiden,p.van.der.plas,a.e.p.veldman}@rug.nl

[2] Department of Ship Hydrodynamics
Technical University of Delft,
Mekelweg 2, 2628 CD Delft, The Netherlands
b.duz@tudelft.nl

Keywords: COMFLOW, VOF, absorbing BC, turbulence regularisation, local grid refinement

Abstract. *The CFD simulation tool* COMFLOW *is developed for the simulation of sloshing liquids and two-phase flow in e.g. offshore applications.* COMFLOW *solves the Navier-Stokes equations in both water and air, with second order accuracy in both space and time. The water surface is advected by means of a modified VOF method, with improved accuracy through a local-height-function (LHF) approach. Numerical reflections are prevented by specially designed absorbing boundary conditions (ABC). Gravity-consistent density averaging for two-phase flow prevents spurious velocities near the free surface.*
Several aspects in the numerical model in COMFLOW *need further extension and improvement. In present research, the focus lies on accurate wave propagation and the effect of viscosity in shear layers (model small-scale flow details). The numerical efficiency is improved by speed-up through local-grid-refinement techniques and parallelisation. Other scientific items that receive attention are multi-dimensional non-reflecting boundary conditions and accurate turbulence modelling on coarse grids with regularisation models.*

1 INTRODUCTION

Wave impact can be a serious threat to the land behind coastal protection structures or the safety on offshore structures, as shown in Fig. 1. Internal sloshing in a vessel may also lead to serious problems, in the worst case even to capsize (of e.g. a LNG carrier). The CFD simulation tool COMFLOW is developed for the simulation of sloshing liquids (two-phase flow) and wave impact, to support the design of structures with enhanced reliability. COMFLOW solves the Navier-Stokes equations in both water and air, with 2nd-order accuracy in both space and time, by means of 2nd-order upwind discretisation in combination with Adams-Bashforth time-stepping. The water surface is advected by means of a modified Volume-of-Fluid (VOF) method, with improved accuracy through a local height-function (LHF) approach, as described below. Compressibility of the air can be included, which is especially important in cases of violent flow conditions, when air entrapment occurs. The employed numerical methods make COMFLOW suitable for accurate predictions of wave impact forces.

Figure 1: Examples of damage because of extreme wave impact.

COMFLOW has been developed initially to study sloshing fuel on board spacecraft in micro-gravity, for which a very accurate and robust description of the free surface is required [6, 15–17, 25, 28]. Later, the methodology was extended to simulations of sloshing liquids and two-phase flow in offshore applications, such as green water loading [10–12, 28], impact loads on fixed structures [3–5, 9–14, 18, 20, 26–28, 32–35] and sloshing tanks [19, 21, 33–38].

To further improve the simulations of wave impact, the COMFLOW3 joint industry project has been set up in cooperation with several companies (oil companies, ship yards, classification institutions, engineering companies, etc.). In COMFLOW3, the focus lies on the accurate simulation of wave propagation, the accurate description of viscous effects in shear layers (model small-scale flow details through regularisation turbulence modelling) and interactive vessel-wave dynamics (include coupling of wave and vessel motion). The numerical efficiency is improved by speed-up through local-grid-refinement techniques and the extension of multi-dimensional non-reflecting boundary conditions.

In this paper, several numerical techniques are described that have been employed succesfully in COMFLOW over the years. Also first results of the COMFLOW3 project are discussed, together with future plans.

2 GOVERNING EQUATIONS

The cushioning effect due to the compressibility of air is important in wave impact simulations. Hence, the governing equations for compressible flow are considered in conservation form (volume Ω, boundary Γ, normal $\vec{n}$). In terms of time t, velocity $\vec{u}=(u,v,w)^T$, pressure p

and fluid density ρ and viscosity μ, conservation of mass and momentum in both water and air are given by

$$\int_\Omega \frac{\partial \rho}{\partial t}\, d\Omega + \oint_\Gamma (\rho \vec{u}) \cdot \vec{n}\, d\Gamma = 0 \tag{1}$$

$$\int_\Omega \frac{\partial (\rho \vec{u})}{\partial t} d\Omega + \oint_\Gamma \rho \vec{u}\, (\vec{u} \cdot \vec{n})\; d\Gamma + \oint_\Gamma p\, \vec{n}\, d\Gamma - \oint_\Gamma \left(\mu \left(\nabla \vec{u} + \nabla \vec{u}^T \right) - \frac{2}{3}\, \mu \nabla \cdot \vec{u} \right) \cdot \vec{n}\, d\Gamma - \int_\Omega \rho \vec{F}\, d\Omega = 0. \tag{2}$$

Note that two-phase flow is described as one aggregated fluid with varying properties ρ and μ. In absence of further external loading, the external force $\vec{F}$ in (2) consists of gravity only. In case of rotating sloshing tanks, the force-term in the equations also contains body forces (e.g. Coriolis force) to account for a rotating reference frame [6, 15–17, 19, 21, 25, 28, 33–38].

The density in a computational cell can be found from the liquid and gas density ρ_l and ρ_g

$$\rho = \frac{F_s}{F_b}\rho_l + \frac{(F_b - F_s)}{F_b}\rho_g, \tag{3}$$

where F_b denotes the fraction of a grid cell open for fluid (consequence of the employed cut-cell approach) and F_s the fraction of that cell filled with liquid. Compressibility of air is included by an adiabatic polytropic equation of state [19, 21, 32–38]

$$\left(\frac{\rho_g}{\rho_{g,0}} \right)^\gamma = \frac{p_g}{p_{g,0}}, \tag{4}$$

with $p_{g,0}$ and $\rho_{g,0}$ the constant atmospheric pressure and ambient gas density, respectively. The coefficient $\gamma = 1.4$ for pure air.

In principle, the free surface follows from $F_s(\vec{x}, t) = 0$, where its motion is given by the advection equation

$$\frac{DF_s}{Dt} = \frac{\partial F_s}{\partial t} + \vec{u} \cdot \nabla F_s = 0. \tag{5}$$

However, in COMFLOW the free surface advection is described through a VOF technique, as described in Section 4.

In case of one-phase flow, a force balance in terms of surface tension σ and mean curvature κ determines a boundary condition at the interface [6, 9–13, 15–17, 25, 28], whereas for two-phase flow an additional body force is obtained [21, 32–38]. A no-slip boundary condition $\vec{u} = 0$ is imposed on the solid walls of e.g. offshore structures or sloshing tanks. The same boundary condition is normally used for the bottom of the computational domain in case of wave simulations. Absorbing boundary conditions (ABC) have been developed for open boundaries (inflow or outflow), see Section 6. In case of incoming waves, the ABC is combined with the prescribed profiles of water heights and velocities.

3 DISCRETISATION

COMFLOW solves the Navier-Stokes equations in both water and air, with 2nd-order accuracy in both space and time, by means of 2nd-order upwind discretisation in combination with Adams-Bashforth time-stepping. The water surface is advected by means of a modified Volume-of-Fluid (VOF) method, with improved accuracy through a local height-function (LHF) approach, as described below. The employed numerical methods make COMFLOW suitable for accurate predictions of the wave impact forces discussed in Section 1.

3.1 Cell labelling method

During a simulation, at every time step, grid cells are given labels to distinguish between fluid, air and boundary. The interior cells containing no fluid ($F_b > 0$ and $F_s = 0$) are labelled as E(mpty) cells. Non-empty cells ($F_s > 0$) adjacent to E cells are labelled as S(urface) cells, as they must contain part of the free surface. All the remaining non-empty cells are labelled F(ull) cells. Cells satisfying $F_s = F_b = 0$ are called B(oundary) cells when they are adjacent to an interior cell, otherwise they are labelled as e(X)terior. In one-phase simulations, E-cells are truly empty and are left out of the computations, with free surface boundary conditions prescribed around S-cells. In two-phase simulations, E-cells contain air and are included in the simulation. In Fig. 2, an example of a label configuration is shown.

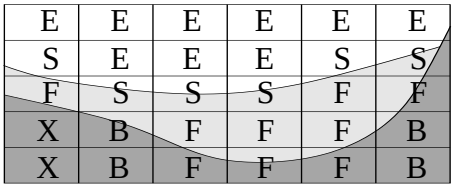

Figure 2: Two dimensional grid-cell labelling for an arbitrary geometry and liquid configuration. Dark and light shading represent solid body and liquid, respectively.

3.2 Discretisation of the Navier-Stokes equations

The equations are coupled through an explicit time-stepping procedure. When first-order Forward Euler (FE) time discretisation (time levels n, time step Δt) is applied to the Navier-Stokes equations (1) and (2) for two-phase flow, several terms arise that require further attention

$$\frac{\rho^{n+1} - \rho^n}{\Delta t} + \rho^n \nabla \cdot \vec{u}^{n+1} + \vec{u}^n \nabla \rho^n = 0 \tag{6}$$

$$\frac{\vec{u}^{n+1} - \vec{u}^n}{\Delta t} + \frac{\vec{u}^n}{\rho^n}\frac{\rho^{n+1} - \rho^n}{\Delta t} + \frac{1}{\rho^n}\nabla \cdot (\rho^n \vec{u}^n \vec{u}^n) + \frac{1}{\rho^n}\nabla p^{n+1}$$
$$-\frac{1}{\rho^n}\nabla\Big(\mu^n\left(\nabla \vec{u}^n + \nabla \vec{u}^{T\,n}\right) - \frac{2}{3}\mu^n \nabla \cdot \vec{u}^n\Big) - \vec{F}^n = 0, \tag{7}$$

The treatment of the unknowns ρ^{n+1}, p^{n+1} at the new time level $n+1$ is described in Section 3.3. The convection term $\frac{1}{\rho^n}\nabla \cdot (\rho^n \vec{u}^n \vec{u}^n)$ is described below. When second-order Adams-Bashforth (AB) time discretisation is used, (6) and (7) will also include the older time level $n-1$.

Spatial discretisation is done on a staggered Cartesian grid, with the pressure located in cell centers and velocities in the middle of cell faces. The convection term $\frac{1}{\rho^n}\nabla \cdot (\rho^n \vec{u}^n \vec{u}^n)$ in (7), which dominates in case of momentum-driven applications, is treated with symmetry-preserving upwind spatial discretisation [30]. With first-order upwind (B2), artificial diffusion is applied to obtain stable solutions, possibly leading to an abundant damping of fluid motion. Using the second-order upwind (B3) scheme, the level of artificial diffusion is much smaller, usually resulting in an acceptable level of damping. B2 can be combined easily with FE, but for B3 an alternative time discretisation is needed to obtain stable solutions, such as AB. The combination of B3 (spatial-) with AB (time-)discretisation makes COMFLOW second order accurate in both space and time. Both combinations FE+B2 and AB+B3 are limited in their stability by the CFL number $\eta = u\Delta t/\Delta x$ and diffusion number $d = 2\mu\Delta t/(\Delta x)^2$. In most

practical cases, convection dominates diffusion, and the CFL number η predominantly controls the stability limit. For the combination B2+FE, the CFL limit is $\eta_{max} \leq 1 - d \approx 1$. For B3+AB this limit is more restrictive: $\eta_{max} \leq \frac{1}{4} - \frac{1}{2}d \approx \frac{1}{4}$. This means that B3+AB requires a four times smaller time step; the price to reduce artificial damping of fluid motion [15–21, 25, 28, 32–38].

3.3 Solving the pressure

The pressure is calculated from a Poisson equation. Taking the divergence of (7) and substitution of the resulting term $\nabla \cdot \vec{u}^{n+1}$ into (6) leads to

$$\Delta t \nabla \cdot \left(\frac{1}{\rho^n} \nabla p^{n+1} \right) = \frac{1}{\rho^n} \frac{\rho^{n+1} - \rho^n}{\Delta t} + \frac{\vec{u}^n}{\rho^n} \cdot \nabla \rho^n + \nabla \cdot \tilde{\vec{u}}^n, \tag{8}$$

with $\tilde{\vec{u}}$ an 'intermediate' velocity, which includes convective, diffusive and force effects. With (3) the unknown density at the new time level ρ^{n+1} is substituted analytically by ρ_g, which gives

$$\Delta t \nabla \cdot \left(\frac{1}{\rho^n} \nabla p^{n+1} \right) = \frac{F_b^n - F_s^n}{F_b^n \rho^n} \left(\frac{\rho_g^{n+1} - \rho_g^n}{\Delta t} + \vec{u}^n \nabla \rho_g^n \right) + \nabla \cdot \tilde{\vec{u}}^n. \tag{9}$$

As a result, occurring density derivatives no longer contain large variations, as they are only determined by compression or expansion of the gas phase. The gas density ρ_g^{n+1} in (9) is subsequently reformulated in p_g through the equation of state (4). The treatment of this term, in combination with the density gradient term, requires more attention and has been described in [19, 21, 32–38]. Finally, p_g is linearised by a Newton approximation to eliminate the exponent $1/\gamma$ and then transferred to the left-hand side of the Poisson equation.

In case of two-phase flow, the entries in the Poisson matrix $\nabla \cdot (\frac{1}{\rho^n} \nabla p^{n+1})$ may differ up to a factor 1000, because of the jumps in ρ^n (water vs. air). Hence, a powerful matrix solver is needed. The Poisson equation is solved with contemporary sparse-matrix techniques, viz. a Krylov subspace method with incomplete LU preconditioning for acceleration. For one-phase flow simulations, the pressure is solved with Successive Over Relaxation (SOR), where the optimal relaxation parameter is adjusted automatically during the iterations [1].

4 ACCURATE FREE-SURFACE DISPLACEMENT

COMFLOW has been developed initially to study sloshing fuel on board spacecraft in microgravity, for which a very accurate and robust description of the free surface is required [6, 15–17, 25, 28]. Later, the methodology was extended to simulations of sloshing liquids and two-phase flow in offshore applications. The Cartesian grid in COMFLOW provides a simple geometrical framework in which the position and slope of the free surface can be accurately described. On unstructured grids the reconstruction of the free-surface is more difficult. The frequently resulting smearing of the free surface erroneously reduces peak pressures and hence leads to less accurate wave-force predictions on unstructured grids.

In COMFLOW, a volume-of-fluid (VOF) method is applied to describe the evolution of the free surface. In principle, the motion of the free surface is described analytically by (5). However, numerically the free surface displacement is done in a different way. First it is reconstructed and then it is advected to the new position. In the employed VOF method, filling rates F_s of individual cells are administrated and fluid fragments are advected with local velocities. The free surface position is subsequently reconstructed from combined fluid volumes contained in single cells. The reconstruction is done with Simple Linear Interface Calculation (SLIC),

where the interface consists of line segments that are constructed either parallel or perpendicular to the major flow axes [7]. A characteristic drawback of SLIC is the unphysical creation of disconnected droplets, resulting from errors in the reconstruction. Moreover, in the original VOF method values are rounded off ($0 \leq F_s \leq 1$) at the end of the displacement algorithm at each time step, leading to significant losses in liquid mass.

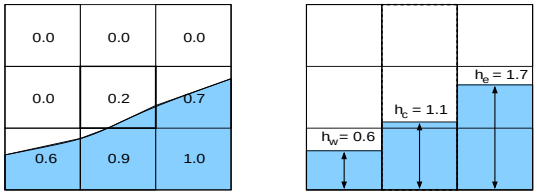

Figure 3: Construction of the LHF around a central S-cell by summing F_s values vertically.

To prevent from isolated droplets and mass losses, a local height function (LHF) has been introduced in COMFLOW [6, 9–13, 15–21, 25, 28, 32–38]. The LHF is applied in a $3 \times 3 \times 3$ block (in 3D) of cells surrounding a central S-cell. First, the orientation of the free surface is determined (horizontal or vertical), depending on the filling rates F_s in the surrounding block of cells. Next, the horizontal or vertical height in each row or column is computed by summing F_s values, see Fig. 3. Based on the LHF, fluid is transported from one cell (donor) to another (acceptor), depending on the magnitude of local velocity, time step and grid sizes. Hence, the interface is explicitly reconstructed through a LHF and subsequently advected. The free-surface at the new time instant is then reconstructed by means of another LHF. The employed technique ensures a sharp interface without smearing, which is essential for accurate simulations of wave impact forces.

In Fig. 4, the liquid configurations after dambreak simulations with and without using LHF are depicted. The LHF approach in COMFLOW clearly results in significantly less erroneous droplets compared to the original VOF method [7] and is strictly mass conserving [9, 11–13, 18–21, 25, 28, 32–38]. The remaining droplets are predominantly located on the tank wall.

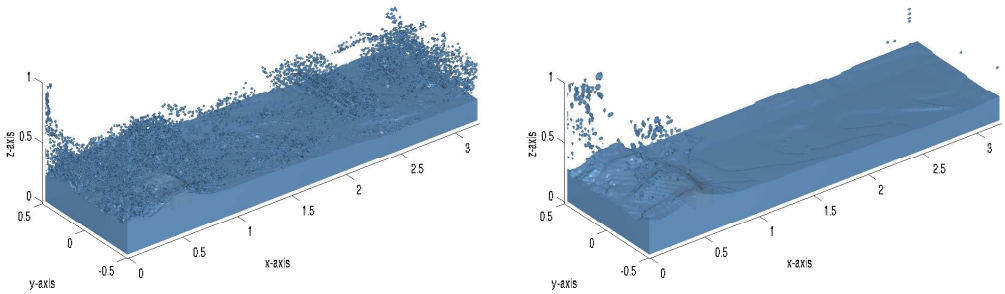

Figure 4: The liquid configurations after a dambreak simulation without (left) and with LHF (right).

When the piecewise linear reconstruction method (PLIC) [39] is used alternatively, in 3D the interface is represented by oblique planes, which is far more difficult to implement. Moreover, the computational costs for the reconstruction of the free surface (esp. the plane constant) are strongly enhanced. Comparison learns that for certain flow applications slightly better results can be obtained, but for many wave-impact and sloshing simulations the present SLIC method with LHF is sufficiently accurate [11]. Nevertheless, recent reconstruction and advection methods are subject of study in the COMFLOW3 project and will probably be used in the future, because of their great potential in accurately simulating wave propagation.

5 GRAVITY-CONSISTENT DENSITY AVERAGING

In case of two-phase flow, the discrete treatment of the density ρ near the free surface is important. For compressible two-phase flow, ρ in the cell center is given by (3), with ρ_g a function of p, which is also located in cell centers. However, as indicated in Fig. 5, ρ is required at velocity locations as well, because of the staggered arrangement of variables. Simple geometrical averaging may result in spurious velocities, especially in case of high density ratios (water vs. air), and eventually cause severe instabilities near the free surface.

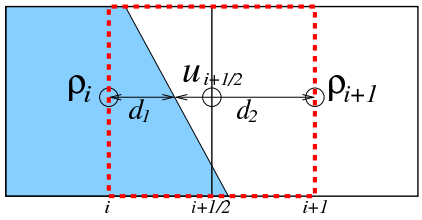

$$\rho_{i+\frac{1}{2}} = \frac{d_1\rho_{i+1} + d_2\rho_i}{d_1 + d_2}$$

Figure 5: The gravity-consistent density average $\rho_{i+1/2}$ is found by weighting ρ_i and ρ_{i+1} with the fraction (coefficients d_1 and d_2) that the free surface splits the red-dashed momentum control volume.

In most of the literature, the spurious currents are damped with suppression techniques (e.g. by adding diffusion). In COMFLOW a superior technique is employed, which can be deduced by considering the momentum equation for a fluid at rest (hydrostatic conditions, zero velocities). This reduces to $\nabla p = \rho\vec{F}$ and hence to $0 = \text{curl}(\rho\vec{F})$, with $\vec{F}$ a body force. This condition should also hold for the discrete variables, otherwise velocity terms in the momentum equation no longer vanish and consequently spurious velocities are generated. This leads to a requirement how ρ should be averaged. Formulas for ρ that satisfy the requirement are called 'gravity consistent', as normally $\vec{F}$ includes gravity. The naive geometrical average $(\rho_i + \rho_{i+1})/2$ is not gravity consistent. A gravity-consistent average is found by looking at the momentum control volume (the red-dashed region in Fig. 5) and weight the neighbouring density values with the fraction that this control volume is split by the free surface [19–21, 27, 33–38].

The difference between simple and sophisticated density averaging for a hydrostatic case is shown in Fig. 6. The effect of the density averaging method on the free surface for a regular sway sloshing experiment (with 10 % filling ratio) is shown in Fig. 7. Naive geometrical averaging clearly results in instabilities, whereas gravity-consistent averaging results in much less disturbances near the free surface.

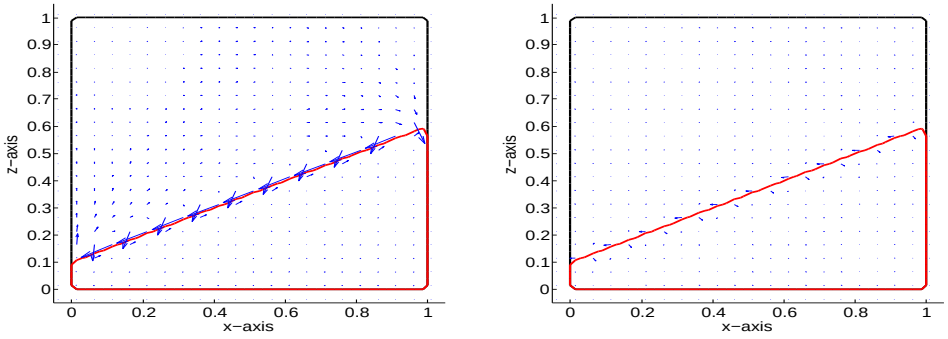

Figure 6: A hydrostatic case, with gravity perpendicular to the free surface. Simple geometrical averaging leads to spurious velocities (left). With gravity-consistent averaging, the free surface stays at rest (right).

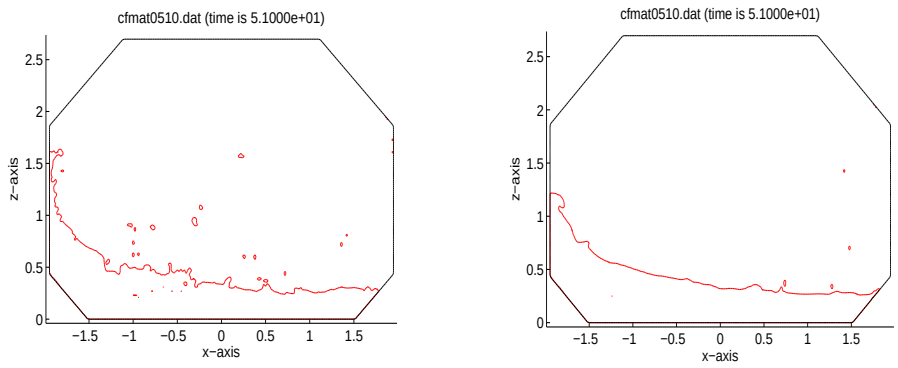

Figure 7: Liquid configurations after simulation of a regular sway sloshing experiment. With gravity-consistent density averaging (right) less instabilities are observed than with simple geometrical averaging (left).

6 ABSORBING BOUNDARY CONDITION (ABC)

For simulations with open boundaries, an ABC has been designed for COMFLOW that suppresses numerical wave reflections from the boundaries. Consequently, open boundaries can be located relatively close to a structure, without influencing outgoing waves or generating numerical reflections that affect water waves inside the flow domain. At the same time, regular or irregular waves can enter the flow domain as prescribed.

6.1 The ABC for 2D waves

The ABC is an extension of the Sommerfeld condition for a potential Φ

$$\left(\frac{\partial}{\partial t} + c^{out}\frac{\partial}{\partial x}\right)\Phi^{out} = 0, \tag{10}$$

which is fully absorbing for one single outgoing wave component with phase velocity c^{out}. However, (10) gives reflections for waves composed of components with other phase velocities $c(kh)$ arriving at the boundary, where kh denotes the dimensionless wave number.

The constant function $c(kh) = c^{out}$ is only a poor approximation of the dispersion relation

$$c(kh) = \sqrt{gh}\sqrt{\frac{\tanh(kh)}{kh}} \approx c^{out}. \tag{11}$$

For the ABC the dispersion relation is highly superiorly approximated by the rational function

$$c(kh) \approx \sqrt{gh}\frac{a_0 + a_1(kh)^2}{1 + b_1(kh)^2}, \tag{12}$$

where the coefficients (a_0,a_1,b_1) are tuned for an optimal approximation over the largest possible range of kh-values. In Fig. 8(left), the reflection coefficients

$$R = \frac{c^{out} - c(kh)}{c^{out} + c(kh)}$$

for (11) and (12) are given, for a range of wave components. The reflection (coefficient) of the ABC is much smaller over a wide range of kh-values.

Because of the e^{-kz}-behaviour of Φ in z-direction, i.e. $k^2\Phi^{out} = \frac{\partial^2}{\partial z^2}\Phi^{out}$, k is replaced by 2nd-order derivatives along the boundary. This leads to the ABC

$$\left[\left(1 + b_1 h^2 \frac{\partial^2}{\partial z^2}\right)\frac{\partial}{\partial t} + \sqrt{gh}\left(a_0 + a_1 h^2 \frac{\partial^2}{\partial z^2}\right)\frac{\partial}{\partial x}\right]\Phi^{out} = 0. \tag{13}$$

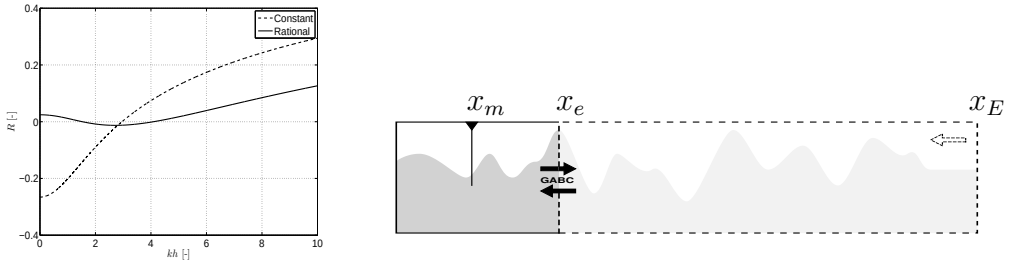

Figure 8: The reflection coefficients of the two approximations of the dispersion relation (left). The two domains used to test the performance of the ABC (right).

The numerical implementation of (13) at an outflow boundary, which coincides with the location of the horizontal velocity u, is described in [18, 20, 32]. In short, first the derivatives of the potential in (13) are formally replaced through $\frac{\partial}{\partial x}\Phi = u$ and $\frac{\partial}{\partial t}\Phi = -p - gz$ (Bernoulli equation). The momentum equation is then used to eliminate the velocity u^{n+1}, which results from $\frac{\partial}{\partial t}$. The final result is a boundary condition for the pressure p, which is easily combined with the internal pressure Poisson equation, but has a larger stencil. Hence, the Poisson equation is more difficult to solve. Even for one-phase flow, a powerful Krylov subspace method is needed with incomplete LU preconditioning for acceleration; the price to reduce spurious reflections.

In [18, 20, 32] the performance of the ABC is investigated by comparing the free surface at a measurement position ($x_m = 200m$) in two simulations, with ABC or Sommerfeld at the outflow ($x_e = 400m$), see Fig. 8(right). As a reference, also a very long domain ($x_E = 2000m$) is considered, where the surface elevation at x_m cannot be disturbed by reflections from the outflow. An ensemble of irregular waves is simulated several wave periods. Any difference at x_m between long and short domain can only be attributed to reflections from the boundary condition at x_e. The performance of the ABC is generally much better than the Sommerfeld condition and accords well with theory. The ABC has also been compared to simulations with a traditional pressure-damping zone technique to prevent wave reflections. An additional free surface pressure p_s is used, proportional to the vertical velocity w at the free surface, which counteracts wave motions. When $w \approx 0$ (long waves), pressure damping is not very effective, unless very long dissipation zones are used. This however significantly adds to the computational effort. The ABC clearly outperforms pressure-damping methods, since both reflections and computing times are considerably smaller [18, 20, 32].

6.2 Extensions of the ABC

The ABC has been demonstrated for 2D waves propagating perpendicular to the open boundary in [18, 20, 32]. In the COMFLOW3 project, the ABC has been extended for waves entering the domain under an angle α and leaving in different directions, as depicted in Fig. 9(left). The ABC (13) has been modified by including direction cosines. Various tests indicate that differences between numerical results and analytical wave profiles are small, for any incoming angle, and for a wide range of wave types. To study wave impact on a structure, COMFLOW users now have two possibilities: keep the position of the structure fixed and vary the incoming angle α, or rotate the structure and keep α constant. Moreover, the COMFLOW user can cut-off the domain at all boundaries, which saves computing time considerably. Again, the reflection is measured from the differences between the small and large domain, see Fig. 9(right). For an incoming 5th-order Stokes wave (with $\alpha = 45^o$), the observed difference is below 2% up to 3 wave periods of simulation time. Further details can be found in [4, 5].

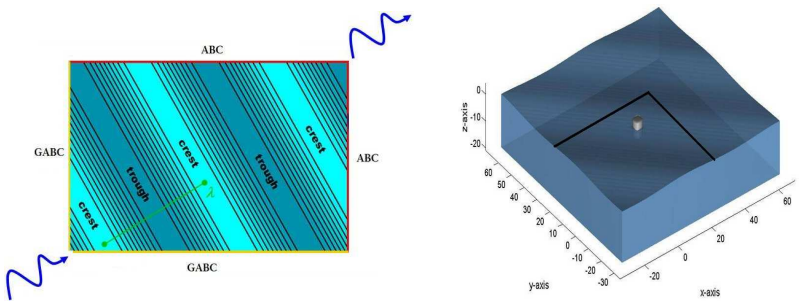

Figure 9: Schematic picture of ABC possibilities (left). All outflow boundaries can be taken close to the structure (right), which saves computing time.

In the future, an even more accurate ABC will be implemented. The ABC will be adapted for non-linear and extreme waves and the effects of stationary currents will be included. For this, the 2nd-order Higdon condition will be considered, i.e.

$$\prod_{j=1}^{2} \left(\frac{\partial}{\partial t} + c_j \frac{\partial}{\partial x} \right) \Phi = 0, \tag{14}$$

which obviously will also include direction cosines. Unfortunately, the Poisson matrix will become more complex (larger stencil) and a dedicated Poisson solver will be employed for computational efficiency.

7 REGULARISATION MODELLING OF VISCOUS EFFECTS

In many practical sloshing applications the role of viscosity is significant. For an accurate prediction of hydrodynamic forces and resistance due to viscous effects, a careful treatment of viscous wall and free shear flow is required. At least the large-scale viscous flow effects should be described accurately. As viscous effects originate from the structure, the discretisation of diffusion near solid walls has been improved. In COMFLOW, a cut-cell approach is used to describe solid geometries, where apertures describe cell volume or face ratios that are open for flow. The discretisation of shear stresses ($\frac{\partial}{\partial y}u$, $\frac{\partial}{\partial x}v$, etc.) has been refined, making careful use of aperture information, following the LS-STAG method [2]. Normal stresses ($\frac{\partial}{\partial x}u$, $\frac{\partial}{\partial y}v$, $\frac{\partial}{\partial z}w$) are discretised analogous to pressure gradients. In 3D roughly 100 cut-cell cases have been considered, which however can be found largely by rotating a few basic cases [23, 24]. Already for simple test cases (e.g. 2D Poiseuille flow) the improvement is clear, as analytical profiles are far more accurately simulated.

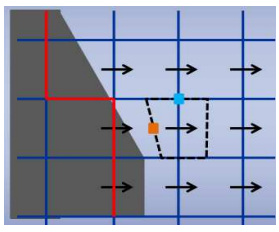

Figure 10: The LS-STAG discretisation of momentum diffusion is based on the deformed momentum control volume (dashed region), making careful use of aperture information.

In many practical applications, turbulence is responsible for a wide range of scales of motion. The required resolution for the smaller scales would lead to excessive computing times.

Therefore, in COMFLOW an 'energy-preserving' turbulence model is implemented, which gives an accurate description of the large scale flow effects, even on coarse grids. The production of small scales is controlled by a special treatment of the convection term, instead of adding eddy-viscosity [31]. It is consistent with the energy-preserving discretisation methods [30] that are already employed in COMFLOW. The regularisation approach modifies the convection term $C(u,u)$ in the Navier-Stokes equations to restrain the production of small scales. A symmetric self-adjoint filter is used to filter the scales below a certain threshold. This leads to a 2nd-order (in filter length) accurate approximation of the convection term $C_2(u,u) = \overline{C(\overline{u},\overline{u})}$, where $\overline{\ }$ means application of the filter. The great virtue of this model is that it conserves important physical quantities (energy, enstrophy, helicity), like the original convection term. Especially energy conservation is crucial for correct prediction of large scale flow. Currently, simple filters are used. The correct implementation and type of filter are still subject of study.

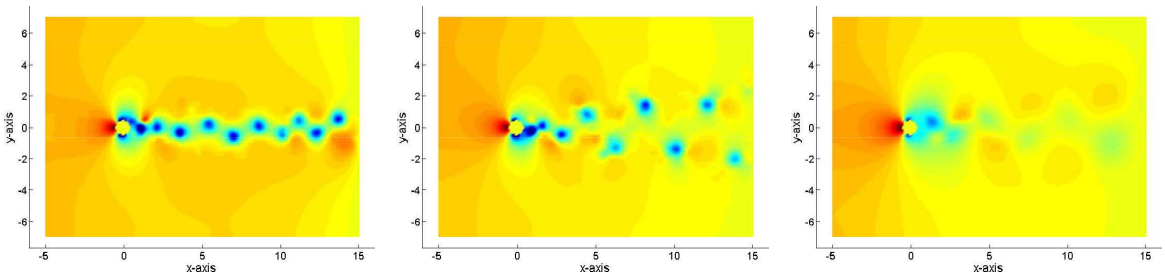

Figure 11: The pressure field during vortex shedding behind a circular cylinder, with pure central discretisation (left), central discretisation with C_2 regularisation (middle) and upwind discretisation (right).

As a test case, the vortex shedding behind a circular cylinder is studied (Re=2000), for 3 different treatments of convection. Close examination of the velocity field shows that with pure central discretisation there are wiggles (well-known numerical artefact) in front of the cylinder and in the vortex region behind. The application of C_2 reduces wiggles, but small erroneous 'wrinkles' are observed in the velocity field. This is currently under investigation. Because of the additional numerical diffusion, in the upwind simulation wiggles are fully suppressed. However, pressure peaks and troughs are not properly predicted, the vortex street is too wide and the additional numerical diffusion results in an overshoot of drag force. The C_2 simulation gives the most realistic wake prediction, as shown in Fig. 11. More details can be found in [23, 24].

In the future, the improved discretisation near solid walls will be investigated further. It will be combined with C_2 regularisation and the approach will be further refined (C_4 regularisation). The near-wall modelling (influence of turbulent boundary layer) will be improved as well, as described in [23,24]. Obviously the turbulence near the free-surface has to be described accurately for a good prediction of hydrodynamic wave loading.

8 LOCAL GRID REFINEMENT (LGR)

As a first step to increase the numerical efficiency, the pressure Poisson solver has been parallelised, since solving the pressure is the far most time-consuming part (up to 95% of the total time) of all the actions to be carried out each time step. Faster Poisson solvers are under consideration and parallelisation of other parts is foreseen. The numerical efficiency is also enhanced by extension of the applicability of the ABC, because of the possibility to reduce the computational domain. With regularisation turbulence models computing time is also saved (relatively), because of the lower need for grid resolution in comparison with LES/RANS models.

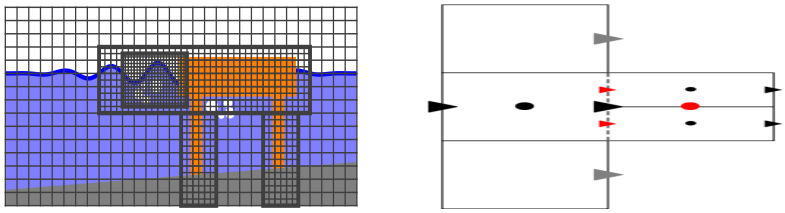

Figure 12: LGR in the simulation of a wave around an offshore structure (left). Discretisation near the refinement involves known (black/grey) and virtual variables (red); cells are split with a 1:2 ratio (right).

In the COMFLOW3 project, the numerical efficiency is further increased through local grid refinement (LGR). For accurate predictions of hydrodynamic forces, generally a high grid resolution is required near the structure. Further away, in less interesting parts of the flow domain, a coarser mesh is usually sufficient. Overall grid stretching leads to cells with unfavourable large aspect ratios. Therefore, in certain parts of the domain cells are split into finer cells (see Fig. 12, left). The data structure in COMFLOW has been modified largely, by adding an additional index to the cell indices (i, j, k), indicating the refinement level. By making clever use of pointers, all existing subroutines can be used without modification. Only for the layers where the actual refinement takes place new subroutines are required, containing e.g. the discretisation of the momentum equations over the 1:2 refinement boundary.

For the discretisation near a grid refinement, special attention is required for the locations of variables. While setting up the discretised Poisson equation, coarse velocities are placed at the interface. The velocity u and pressure gradient $\frac{\partial}{\partial x}p$ are taken constant on the coarse cell face, similar to the ideas presented in [22]. Missing variables (see Fig. 12, right) are found from interpolation. As a result, a compact scheme is found for the pressure equation, with 1st-order accuracy. Simple test cases (Couette flow, Poiseuille flow) indicate that errors are generally very small. Only at subgrid corners little deviation from the analytical solutions is found, which will be investigated further in the future. In Fig. 13, the flow around a circular cylinder is considered, with two levels of grid refinement near the cylinder. The snapshots of pressure and vorticity show that the flow goes through the refinement layers without disturbance. More details can be found in [23, 24].

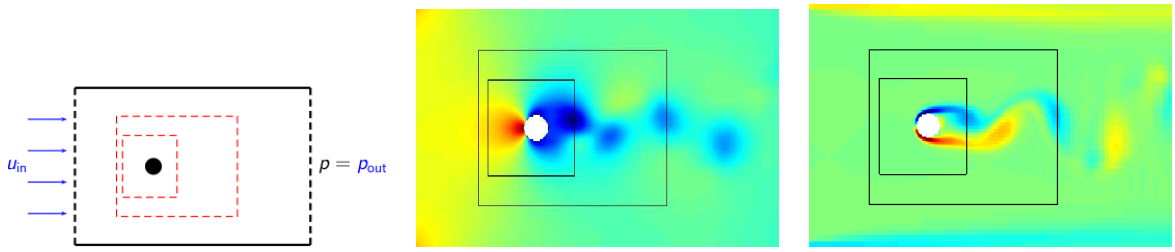

Figure 13: Local grid refinement for the flow around a circular cylinder ($D = 1\,m$, $U_{in} = 1.0\,m/s$, $Re = 100$). Schematic overview of setup (left), computed pressure distribution (middle) and vorticity (right).

Advection of the free surface through refinement boundaries is currently investigated. The advection algorithm has been adjusted to the local changes in grid structure. Moreover, the LHF has been modified near the refinement, to get the correct F_s-sums in horizontal/vertical layers and hence the correct orientation of the free surface. First tests indicate that the disturbance is small when the free surface moves predominantly perpendicularly through the refinement. For other cases, first the pressure boundary condition near the free-surface has to be adapted.

9 INTERACTIVE BODY MOTION (IBM)

The first application of IBM with COMFLOW was the interaction between internal liquid sloshing and overall spacecraft dynamics. Experiments in space with the Sloshsat FLEVO satellite were supported by COMFLOW simulations [6, 15–17, 25, 28] (see Fig. 14, left). The Navier-Stokes equations for the fluid and the equations for solid-body dynamics were directly coupled and solved simultaneously. The influence of the moving fluid was accounted for by computing the variable centre of mass, moment of inertia and (pressure and viscous) forces on the tank wall every time step. The interaction between water waves and mechanical anchor constructions was studied with the Statoil Snorre tension leg platform (TLP) (see Fig. 14, right), where the mechanical motion algorithm and the flow solver were also strongly intertwined [8].

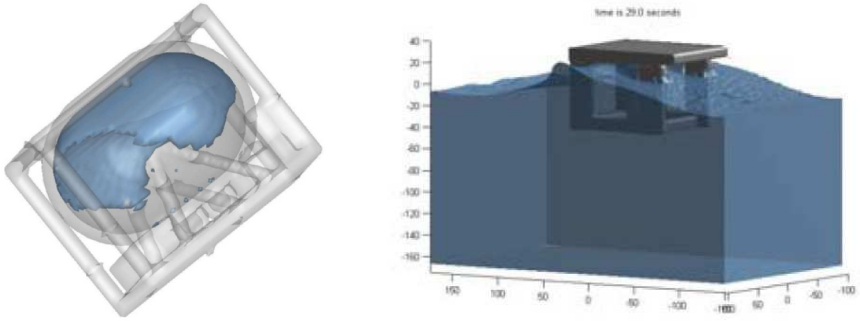

Figure 14: Examples of IBM studies with COMFLOW: Sloshsat FLEVO (left) and Statoil Snorre TLP (right).

Unfortunately, direct coupling is not always possible, e.g. when COMFLOW is coupled to a commercial structural code (black box). However, a strong coupling is normally required for stability in case of large mass and inertia ratios. In the future, the quasi-simultaneous approach [29] will be implemented in COMFLOW. In this method, a simple approximation of the mechanical model is implemented as a preconditioner, to enhance convergence of the iterations between fluid and body. This usually provides sufficient stability of the coupling, also when the exact dynamical model is applied in the second step.

10 CONCLUSIONS

The CFD simulation tool COMFLOW is developed for the accurate simulation of two-phase flow and wave impact in e.g. offshore applications. Over the years, several numerical techniques have been developed using COMFLOW. A number of proven techniques have been presented: ABC to minimise numerical reflections from open boundaries, LHF for accurate free-surface displacement and gravity-consistent density averaging for two-phase flow to prevent spurious velocities near the free surface.

Several first steps and future plans to enlarge the functionality of COMFLOW have been discussed. The ABC has been extended for incoming and outgoing waves under an angle. The effect of viscosity in shear layers is more accurately described through regularisation turbulence modelling and improved discretisation of diffusion. With LGR the numerical efficiency has been increased. In the future the focus is on (propagation of) extreme waves and further improvement of both regularisation modelling and LGR. Also interactive vessel-wave dynamics will be subject of study.

Acknowledgement

The research and development of COMFLOW are supported by the Dutch Technology Foundation STW, applied science division of NWO and the technology program of the Ministry of Economic Affairs in The Netherlands.

REFERENCES

[1] E.F.F. Botta, M.H.M. Ellenbroek: A modified SOR method for the Poisson equation in unsteady free-surface flow calculations. *J. Comp. Phys.*, 60:119–134, 1985.

[2] Y. Cheny, O. Botella: The LS-STAG method: A new immersed boundary/level-set method for the computation of incompressible viscous flows in complex moving geometries with good conservation properties. *J. Comp. Phys.*, 229:1043–1076, 2010.

[3] D.G. Danmeier, R.K.M. Seah, T. Finnigan, D. Roddler, A. Abault, M. Vache, J.T. Imamura: Validation of wave run-up calculation methods for a gravity based structure. In *27th Int. Conf.*, 2008. OMAE2008-57625.

[4] B. Duz, R.H.M. Huijsmans, A.E.P. Veldman, M.J.A. Borsboom, P.R. Wellens: An absorbing boundary condition for regular and irregular wave simulations. In *V Int. Conf.*, 2011. MARINE 2011.

[5] B. Duz, R.H.M. Huijsmans, P.R. Wellens, M.J.A. Borsboom, A.E.P. Veldman: Towards a general-purpose open boundary condition for wave simulations. In *30th Int. Conf.*, 2011. OMAE2011-49979.

[6] J. Gerrits, A.E.P. Veldman: Dynamics of Liquid-Filled Spacecraft. *J. Eng. Math.*, 45:21–38, 2003.

[7] C.R. Hirt, B.D. Nichols: Volume Of Fluid (VOF) Method for the Dynamics of Free Boundaries. *J. Comp. Phys.*, 39:201–225, 1981.

[8] T.B. Johannessen, S. Haver, T. Bunnik, B. Buchner: Extreme wave effects on deep water TLP's. In *Proc. Deep Offshore Techn. 2006*, 2006.

[9] K.M.T. Kleefsman, A.E.P. Veldman: An improved Volume-Of-Fluid method for wave impact. In *4th Eur. Congr.* ECCOMAS, 2004.

[10] K.M.T. Kleefsman, G. Fekken, A.E.P. Veldman, B. Buchner, T. Bunnik, B. Iwanowski: Prediction of green water and wave loading using a Navier-Stokes based simulation tool. In *21st Int. Conf.*, 2002. OMAE2002-28480.

[11] K.M.T. Kleefsman, G. Fekken, A.E.P. Veldman, B. Iwanowski, B. Buchner: A Volume Of Fluid Based Simulation Method for Wave Impact Problems. *J. Comp. Phys.*, 206(1):363–393, 2005.

[12] K.M.T. Kleefsman, G.E. Loots, A.E.P. Veldman, B. Buchner, T. Bunnik, E. Falkenberg: The numerical solution of green water loading including vessel motions and the incoming wave field. In *24th Int. Conf.*, 2005. OMAE2005-67448.

[13] K.M.T. Kleefsman, A.E.P. Veldman, T. Bunnik: An improved Volume-Of-Fluid (IVOF) method for wave impact type problems. In *Spec. Symp. on FPSO Integrity*, 2004. OMAE-FPSO04-0066.

[14] R. Luppes, B. Duz, H.J.L. van der Heiden, P. van der Plas, A.E.P. Veldman: Numerical simulation of extreme wave impact on offshore platforms and coastal constructions. In *V Int. Conf.*, 2011. MARINE 2011.

[15] R. Luppes, J.A. Helder, A.E.P. Veldman: Liquid sloshing in microgravity. In *56th Int. Astr. Congr.* IAF, 2005. IAF-05-A2.2.07.

[16] R. Luppes, J.A. Helder, A.E.P. Veldman: The numerical simulation of liquid sloshing in microgravity. In *Eur. Conf.* ECCOMAS CFD, 2006. ISBN 909020970-0, paper490.

[17] R. Luppes, J.A. Helder, A.E.P. Veldman: The numerical simulation of liquid sloshing in microgravity. In *Computational Fluid Dynamics 2006*, pages 607–612. ICCFD, 2009. doi: 10.1007/978-3-540-92779-2-95.

[18] R. Luppes, A.E.P. Veldman, P.R. Wellens: Absorbing Boundary Conditions for Wave Simulations around Offshore Structures. In *Eur. Conf.* ECCOMAS CFD, 2010.

[19] R. Luppes, A.E.P. Veldman, R. Wemmenhove: Simulation of two-phase flow in sloshing tanks. In *Computational Fluid Dynamics 2010*, pages 555–561. ICCFD, 2010. ISBN: 9783642178832.

[20] R. Luppes, P.R. Wellens, A.E.P. Veldman, T. Bunnik: CFD simulations of wave run-up against a semi-submersible with absorbing boundary conditions. In *Int. Conf.*, 2009. MARINE 2009.

[21] R. Luppes, R. Wemmenhove, A.E.P. Veldman, T. Bunnik: Compressible Two-Phase Flow in Sloshing Tanks. In *5th Eur. Congr.* ECCOMAS, 2008.

[22] E. Uzgoren, R. Singh, J. Sim, W. Shyy: Computational modeling for multiphase flows with spacecraft application. *Progr. in Aerospace Sc.*, 43(4-6):138–192, 2007.

[23] H.J.L. van der Heiden, van der PlasP., A.E.P. Veldman, R. Luppes, R.W.C.P. Verstappen: Efficiently Modeling Viscous Flow Effects by means of Regularization Turbulence Modeling and Local Grid Refinement. In *Computational Fluid Dynamics 2012*. ICCFD, 2012. paper ICCFD7-2504.

[24] P. van der Plas, H.J.L. van der Heiden, A.E.P. Veldman, R. Luppes, R.W.C.P. Verstappen: Efficiently simulating viscous flow effects by means of regularization turbulence modeling and local grid refinement. In *Eur. Conf.* ECCOMAS CFD, 2012. paper 1474.

[25] A.E.P. Veldman, J. Gerrits, R. Luppes, J.A. Helder, J.P.B. Vreeburg: The numerical simulation of liquid sloshing on board spacecraft. *J. Comp. Phys.*, 224:82–99, 2007.

[26] A.E.P. Veldman, K.M.T. Kleefsman, G. Fekken: Numerical computation of wave impact. In *Int. Conf.*, pages 323–332, 2005. MARINE 2005.

[27] A.E.P. Veldman, R. Luppes, T. Bunnik, R.H.M. Huijsmans, B. Duz, B. Iwanowski, R. Wemmenhove, M.J.A. Borsboom, P.R. Wellens, H.J.L. van der Heiden, P. van der Plas: Extreme wave impact on offshore platforms and coastal constructions. In *30th Int. Conf.*, 2011. OMAE2011-49488.

[28] A.E.P. Veldman: The simulation of violent free-surface dynamics at sea and in space. In *Eur. Conf.* ECCOMAS CFD, 2006. ISBN 909020970-0, paper 492.

[29] A.E.P. Veldman: A simple interaction law for viscous-inviscid interaction. *J. Eng. Math.*, 65:367–383, 2009.

[30] R.W.C.P. Verstappen, A.E.P. Veldman: Symmetry-Preserving Discretisation of Turbulent Flow. *J. Comp. Phys.*, 187:343–368, 2003.

[31] R.W.C.P. Verstappen: On restraining the production of small scales of motion in a turbulent channel flow. *Comp. Fluids*, 37:887–897, 2008.

[32] P.R. Wellens, R. Luppes, A.E.P. Veldman, M.J.A Borsboom: CFD simulations of a semi-submersible with absorbing boundary conditions. In *28th Int. Conf.*, 2009. OMAE2009-79342.

[33] R. Wemmenhove, G.E. Loots, A.E.P. Veldman: Hydrodynamic wave loading on offshore structures simulated by a two-phase flow model. In *25th Int. Conf.*, 2006. OMAE2006-92253.

[34] R. Wemmenhove, G.E. Loots, A.E.P. Veldman: Numerical simulation of hydrodynamic wave loading by a two-phase model. In *Eur. Conf.* ECCOMAS CFD, 2006. ISBN 909020970-0, paper 517.

[35] R. Wemmenhove, G.E. Loots, R. Luppes, A.E.P. Veldman: Modeling two-phase flow with offshore applications. In *24th Int. Conf.*, 2005. OMAE2005-67460.

[36] R. Wemmenhove, R. Luppes, A.E.P. Veldman, T. Bunnik: Numerical simulation and model experiments of sloshing in LNG tanks. In *Int. Conf.*, 2007. MARINE 2007.

[37] R. Wemmenhove, R. Luppes, A.E.P. Veldman, T. Bunnik: Numerical Simulation of Sloshing in LNG Tanks with a Compressible Two-Phase Model. In *26th Int. Conf.*, 2007. OMAE2007-29294.

[38] R. Wemmenhove, R. Luppes, A.E.P. Veldman, T. Bunnik: Application of a VOF Method to Model Compressible Two-Phase Flow in Sloshing Tanks. In *27th Int. Conf.*, 2008. OMAE2008-57254.

[39] D.L. Youngs: Time-dependent multi-material flow with large fluid distortion. In K. W. Morton and M. J. Baine, editors, *Numerical Methods for Fluid Dynamics*, pages 273–285. Academic Press, New York, 1982.